

HCR spectral imaging: 10-plex, quantitative, high-resolution RNA and protein imaging in highly autofluorescent samples

Samuel J. Schulte¹, Mark E. Fornace¹, John K. Hall¹, Grace J. Shin¹ and Niles A. Pierce^{1,2,*}

ABSTRACT

Signal amplification based on the mechanism of hybridization chain reaction (HCR) provides a unified framework for multiplex, quantitative, high-resolution imaging of RNA and protein targets in highly autofluorescent samples. With conventional bandpass imaging, multiplexing is typically limited to four or five targets owing to the difficulty in separating signals generated by fluorophores with overlapping spectra. Spectral imaging has offered the conceptual promise of higher levels of multiplexing, but it has been challenging to realize this potential in highly autofluorescent samples, including whole-mount vertebrate embryos. Here, we demonstrate robust HCR spectral imaging with linear unmixing, enabling simultaneous imaging of ten RNA and/or protein targets in whole-mount zebrafish embryos and mouse brain sections. Further, we demonstrate that the amplified and unmixed signal in each of the ten channels is quantitative, enabling accurate and precise relative quantitation of RNA and/or protein targets with subcellular resolution, and RNA absolute quantitation with single-molecule resolution, in the anatomical context of highly autofluorescent samples.

KEY WORDS: RNA fluorescence *in situ* hybridization, RNA-FISH, Immunofluorescence, qHCR imaging, dHCR imaging, Whole-mount zebrafish embryos, Mouse brain sections

INTRODUCTION

RNA *in situ* hybridization methods (Harrison et al., 1973; Tautz and Pfeifle, 1989; Qian et al., 2004) and immunohistochemistry methods (Coons et al., 1941; Ramos-Vara, 2005; Kim et al., 2016) provide biologists with essential tools for elucidating the spatial organization of biological circuitry, enabling imaging of RNA and protein expression in an anatomical context. When developing these technologies for use in a given sample type, the first priority is to achieve a high signal-to-background ratio when mapping the expression pattern of a single target RNA or protein. Once this prerequisite has been met, other important priorities include the need for multiplex experiments to map relationships between circuit elements within a single specimen, the preference for the signal to be quantitative rather than qualitative, and the desire

for the staining to be high-resolution to enable examination of spatial relationships at a subcellular level. In thin samples with low autofluorescence, it is straightforward to achieve all of these goals using probes direct-labeled with fluorophores (Kislauskis et al., 1993; Femino et al., 1998; Kosman et al., 2004; Chan et al., 2005; Raj et al., 2008). However, in whole-mount vertebrate embryos and other challenging imaging settings including thick brain slices, autofluorescence greatly increases the technical challenge of achieving high signal-to-background, motivating the development of *in situ* amplification methods (Qian et al., 2004; Ramos-Vara and Miller, 2014). For decades, the challenge of achieving high signal-to-background in thick autofluorescent samples proved sufficiently daunting that it was predominantly met by using enzyme-mediated catalytic reporter deposition (CARD) for both *in situ* hybridization (Tautz and Pfeifle, 1989; Harland, 1991; Lehmann and Tautz, 1994; Kerstens et al., 1995; Nieto et al., 1996; Thisse et al., 2004; Piette et al., 2008; Thisse and Thisse, 2008; Wang et al., 2012) and immunohistochemistry (Takakura et al., 1997; Sillitoe and Hawkes, 2002; Ahnfelt-Rønne et al., 2007; Fujisawa et al., 2015; Staudt et al., 2015), which came with unfortunate consequences. Using CARD, multiplexing is cumbersome owing to the lack of orthogonal deposition chemistries, necessitating serial amplification for one target after another (Denkers et al., 2004; Kosman et al., 2004; Clay and Ramakrishnan, 2005; Barroso-Chinea et al., 2007; Tóth and Mezey, 2007; Glass et al., 2009; Mitchell et al., 2014; Stack et al., 2014; Tsujikawa et al., 2017), staining is qualitative rather than quantitative, and spatial resolution is routinely compromised by diffusion of reporter molecules prior to deposition (Tautz and Pfeifle, 1989; Takakura et al., 1997; Sillitoe and Hawkes, 2002; Thisse et al., 2004; Acloque et al., 2008; Weiszmänn et al., 2009). Notably, cumbersome serial multiplexing leads to progressive sample degradation and lengthy protocols. For example, it takes 4 days for 2-plex imaging in whole-mount zebrafish embryos (Thisse et al., 2004; Clay and Ramakrishnan, 2005) and 5 days for 3-plex imaging in whole-mount chicken embryos (Denkers et al., 2004; Acloque et al., 2008).

To overcome these longstanding shortcomings of CARD in the context of RNA imaging, *in situ* amplification based on the mechanism of hybridization chain reaction (HCR) (Dirks and Pierce, 2004) draws on principles from the emerging discipline of dynamic nucleic acid nanotechnology to enable multiplex, quantitative, high-resolution RNA fluorescence *in situ* hybridization (RNA-FISH) with high signal-to-background in highly autofluorescent samples (Choi et al., 2010, 2014, 2016, 2018; Shah et al., 2016a; Trivedi et al., 2018). Using HCR RNA-FISH, targets are detected using probes that trigger isothermal, enzyme-free chain reactions in which fluorophore-labeled HCR hairpins self-assemble into tethered fluorescent amplification polymers, boosting the signal above autofluorescence. The programmability of HCR allows orthogonal amplifiers to operate independently within the sample so that the experimental timeline for multiplex experiments is

¹Division of Biology & Biological Engineering, California Institute of Technology, Pasadena, CA 91125, USA. ²Division of Engineering & Applied Science, California Institute of Technology, Pasadena, CA 91125, USA.

*Author for correspondence (niles@caltech.edu)

ORCID: S.J.S., 0000-0001-9982-6504; M.E.F., 0000-0002-5829-5839; J.K.H., 0009-0005-5120-5940; G.J.S., 0009-0004-7778-6328; N.A.P., 0000-0003-2367-4406

This is an Open Access article distributed under the terms of the Creative Commons Attribution License (<https://creativecommons.org/licenses/by/4.0/>), which permits unrestricted use, distribution and reproduction in any medium provided that the original work is properly attributed.

Handling Editor: Benoît Bruneau
Received 31 August 2023; Accepted 21 December 2023

independent of the number of target RNAs (Choi et al., 2010, 2014). The amplified HCR signal scales approximately linearly with the number of target molecules, enabling accurate and precise RNA relative quantitation with subcellular resolution in an anatomical context (Choi et al., 2018; Trivedi et al., 2018). Amplification polymers remain tethered to their initiating probes, preventing the signal from diffusing away from the target, enabling imaging of RNA expression with subcellular or single-molecule resolution as desired (Choi et al., 2014, 2016, 2018; Shah et al., 2016a). Building on these advances, HCR immunofluorescence (IF) extends the benefits of HCR signal amplification to protein imaging (Schwarzkopf et al., 2021), enabling accurate and precise protein relative quantitation with subcellular resolution in highly autofluorescent samples, including formalin-fixed, paraffin-embedded (FFPE) tissue sections. Moreover, simultaneous HCR RNA-FISH/IF provides a unified framework for multiplex, quantitative, high-resolution RNA and protein imaging in highly autofluorescent samples with one-step HCR signal amplification performed for all target RNAs and proteins simultaneously (Schwarzkopf et al., 2021).

With conventional bandpass fluorescence imaging, fluorescence is excited with a light source for each channel (e.g. a laser) and collected as a single intensity using a different bandpass filter for each channel. Fluorescence microscopes are typically able to distinguish at most four or five fluorophores using bandpass imaging owing to overlapping spectra for different fluorophores (e.g. see Fig. 1A). Higher levels of multiplexing can be achieved by

repeated staining, imaging, registration and stripping (Lignell et al., 2017; Kishi et al., 2019; Koh et al., 2019; Saka et al., 2019; Kennedy-Darling et al., 2021; Ghoddousi et al., 2022), but these approaches are unfavorable for whole-mount embryos (which are difficult to immobilize on a slide to facilitate registration between imaging rounds) and for delicate specimens (which degrade during repeated staining and stripping rounds). Even higher levels of multiplexing can be achieved using temporal barcoding methods (Lubeck et al., 2014; Chen et al., 2015; Moffitt et al., 2016; Shah et al., 2016b), which likewise exploit repeated staining, imaging, registration and stripping (with the accompanying restrictions on sample type), but barcoding methods additionally place restrictions on the targets, requiring low target expression levels in order to spatially separate the signal for each target molecule as a distinct dot. Spectral imaging (Garini et al., 2006; Mansfield et al., 2008; Valm et al., 2016) offers a strategy for exceeding 5-plex without the need for repeated staining, imaging, registration and stripping, and without constraints on target expression level or pattern. However, in practice, it has proven difficult to realize the conceptual promise to move beyond five targets in the challenging imaging environment of whole-mount vertebrate embryos (Cutrale et al., 2017; Cutrale et al., 2019).

With spectral imaging, each fluorophore is excited by one or more lasers and fluorescence is collected with one or more detectors, generating a signal for each pixel that is a superposition of fluorescence from multiple fluorophores, characterized for multiple

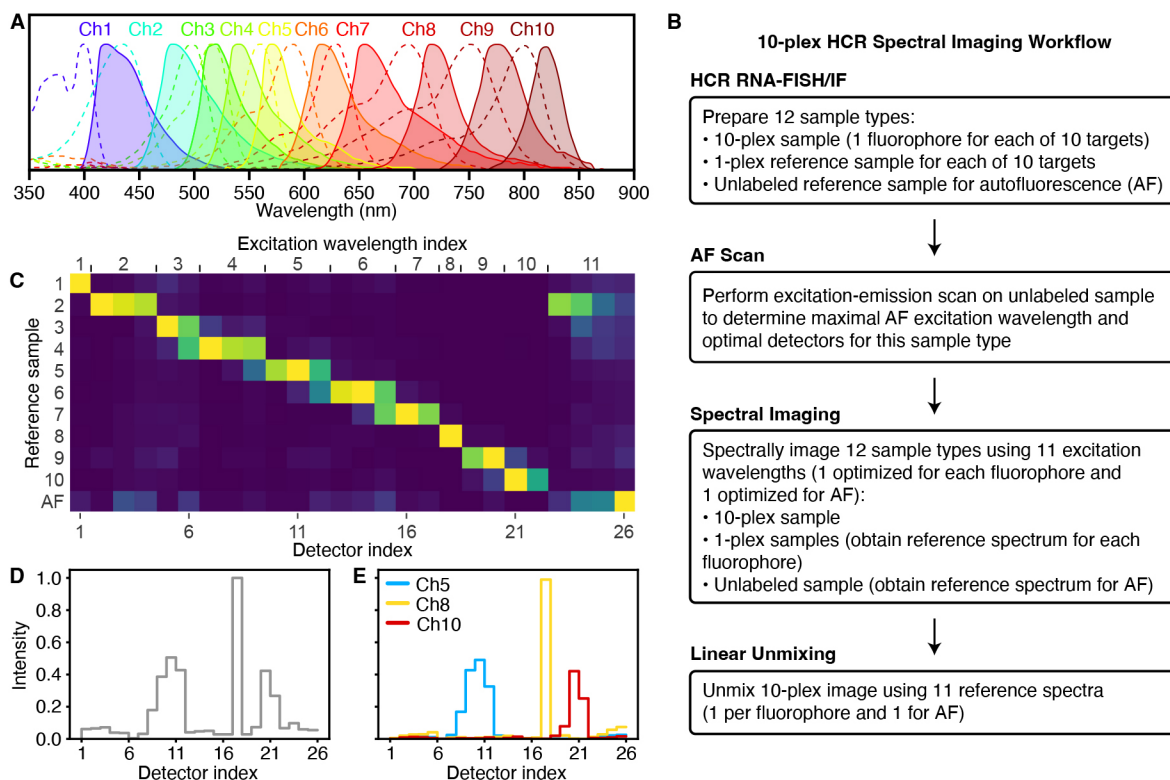


Fig. 1. Overview of 10-plex HCR spectral imaging and linear unmixing. (A) Excitation spectra (dashed lines) and emission spectra (solid lines) for the ten fluorophores selected for HCR spectral imaging (left to right: Alexa405, Atto425, Alexa488, Alexa514, Alexa546, Alexa594, Atto633, Alexa700, Alexa750, iFluor800; spectra from FluoroFinder). (B) Workflow for performing a 10-plex HCR spectral imaging and linear unmixing experiment. (C) Linear unmixing matrix of normalized reference spectrum intensities gathered via spectral imaging of ten fluorophores in 1-plex samples and autofluorescence (AF) in an unlabeled sample for 27 hpf zebrafish embryos. (D) Spectral fluorescence intensities for a single pixel in the notochord of a 27 hpf zebrafish embryo. (E) Linear unmixing of the pixel fluorescence shown in D using the reference spectra from C to determine the fluorescence contribution of each fluorophore and AF, revealing that the fluorescence in this notochord pixel is predominantly a combination of Ch5, Ch8 and Ch10 fluorophores.

excitation wavelengths using multiple detectors at different emissions wavelengths (Garini et al., 2006). Spectrally imaging a set of reference samples that each contain only one type of fluorophore provides a reference spectrum for each channel. Each pixel in a spectral image of the sample of interest may then be interpreted as a linear superposition of these reference spectra with an unknown coefficient for each channel. Linear unmixing of the fluorescence in that pixel then determines the non-negative coefficients that best approximate the spectrum of the sample of interest, revealing the fluorescence contribution of each channel (Mansfield et al., 2008). The output of linear unmixing is a set of unmixed fluorescence channels for all pixels. The mathematics of spectral imaging are enticing, hypothetically enabling separation of an arbitrary number of fluorophore channels, but the imperfections and complexities of real-world samples and experiments have so far undermined the practicality of spectral imaging in whole-mount vertebrate embryos. Here, we establish standardized ingredients and workflows for HCR spectral imaging to enable biologists to perform robust 10-plex imaging of RNA and protein targets in whole-mount vertebrate embryos and other highly autofluorescent samples in a plug-and-play manner. Moreover, we demonstrate that HCR spectral imaging and linear unmixing generate high signal-to-background, quantitative signal, and high resolution in all ten channels.

RESULTS

Ingredients and workflow for robust 10-plex HCR spectral imaging

Using 10-plex HCR spectral imaging, each of ten targets is detected using a different probe set comprising one or more probes capable of triggering a different HCR amplifier carrying a different fluorophore. Our approach combines several ingredients into a standardized workflow. First, an optimized set of ten orthogonal HCR amplifiers (one per target) that operate independently in the same sample at the same time. The role of these amplifiers is to boost the signal strength relative to autofluorescence in each channel, increasing the ease and robustness of linear unmixing, and ultimately the signal-to-background of the unmixed channels. Second, an optimized set of ten fluorophores (one per HCR amplifier) with overlapping excitation and emission spectra selected to facilitate subsequent linear unmixing (spectra depicted in Fig. 1A). Third, an optimized set of excitation wavelengths (one per fluorophore; see Table S5) and an optimized set of detection wavelengths (using between one and three detectors per fluorophore; see Table S5). Fourth, an optimized excitation wavelength and set of detection wavelengths for autofluorescence, which is treated as an 11th channel; the optimized excitation and emission values for autofluorescence will need to be determined for a given sample type by the user in a preliminary experiment as described below. Fifth, spectral imaging hardware that provides the flexibility to use optimal excitation wavelengths for each fluorophore and for autofluorescence; we use the Leica Stellaris 8 confocal microscope, which is equipped with a tunable white-light laser capable of generating laser lines in 1 nm increments between 440 nm to 790 nm (in addition to a fixed 405 nm laser). Sixth, a linear unmixing algorithm that takes as input a 10-plex spectral image and 11 reference spectra (one per fluorophore and one for autofluorescence) and returns as output 11 unmixed channels (one per fluorophore and one for autofluorescence); we use either the Leica LAS X software or our own Unmix 1.0 software package.

These ingredients are employed in a standardized workflow (see Fig. 1B) to perform robust 10-plex HCR spectral imaging of ten

RNA and/or protein targets. First, the user prepares 12 sample types: a 10-plex sample (or multiple replicate samples as desired), a 1-plex reference sample for each of ten targets, and two unlabeled autofluorescence (AF) samples (one for an excitation-emission scan and one AF reference sample). Second, the user employs one AF sample to perform an excitation-emission scan to determine the excitation wavelength that maximizes autofluorescence, which in turn determines a set of optimized detection wavelengths (using four detectors); this preliminary step need not be repeated for future experiments in the same sample type. Third, the user spectrally images the 10-plex sample using the standardized set of 11 excitation wavelengths (one optimized for each fluorophore and one optimized for AF). Likewise, the user spectrally images each 1-plex reference sample using the 11 standardized excitation wavelengths to obtain a reference spectrum for each fluorophore in a region of maximum expression for a given target. Further, the user spectrally images the AF reference sample using the 11 standardized excitation wavelengths to obtain a reference spectrum for AF in a region of maximum autofluorescence. Fourth, the 11 reference spectra (one per fluorophore and one for AF) are used to linearly unmix the 10-plex image and produce 11 unmixed channels (one per fluorophore and one for AF).

As an example, Fig. 1C depicts 11 reference spectra (one per fluorophore and one for autofluorescence) collected in a whole-mount zebrafish embryo. Each reference sample was excited with 11 different excitation wavelengths (standardized ingredients of the method) and for each excitation wavelength, emissions were collected with between one and four detectors (a total of 26 detectors spanning the range of emissions wavelengths; also standardized ingredients of the method). From a spectral image of the 10-plex sample, Fig. 1D depicts the raw spectral fluorescence intensities for a single pixel in the notochord region of a whole-mount zebrafish embryo collected using 11 excitation wavelengths and a total of 26 detectors. Linear unmixing determines the (non-negative) contributions from each of the ten fluorophores and AF (treated as an 11th channel), which combine to create the spectral fluorescence intensity curve. Fig. 1E shows that the fluorescence in this notochord pixel is predominantly a combination of channel (Ch) 5, Ch8 and Ch10 fluorophores, which together generate the three peaks seen in the spectral fluorescence intensity curve of Fig. 1D.

10-plex RNA imaging using spectral HCR RNA-FISH in a whole-mount vertebrate embryo

We first validated 10-plex HCR spectral imaging for HCR RNA-FISH, which is performed using the two-stage protocol summarized in Fig. 2A. During the detection stage, an RNA target is detected using a probe set comprising one or more pairs of split-initiator DNA probes, each carrying a fraction of HCR initiator i1 (Choi et al., 2018). Probe pairs that hybridize specifically to proximal binding sites on the target RNA colocalize a full HCR initiator i1 capable of triggering HCR signal amplification. Meanwhile, any individual probes that bind nonspecifically in the sample do not colocalize full HCR initiator i1 and do not trigger HCR. During the amplification stage, each colocalized full HCR initiator i1 triggers self-assembly of metastable fluorophore-labeled HCR hairpins (h1 and h2) into a tethered fluorescent HCR amplification polymer to generate an amplified signal at the site of the target RNA. For 10-plex HCR spectral imaging, the same two-stage protocol is used as for a 1-plex experiment, with all ten targets detected in parallel during the detection stage, and signal amplification performed for all ten targets in parallel during the amplification stage (Fig. 2B).

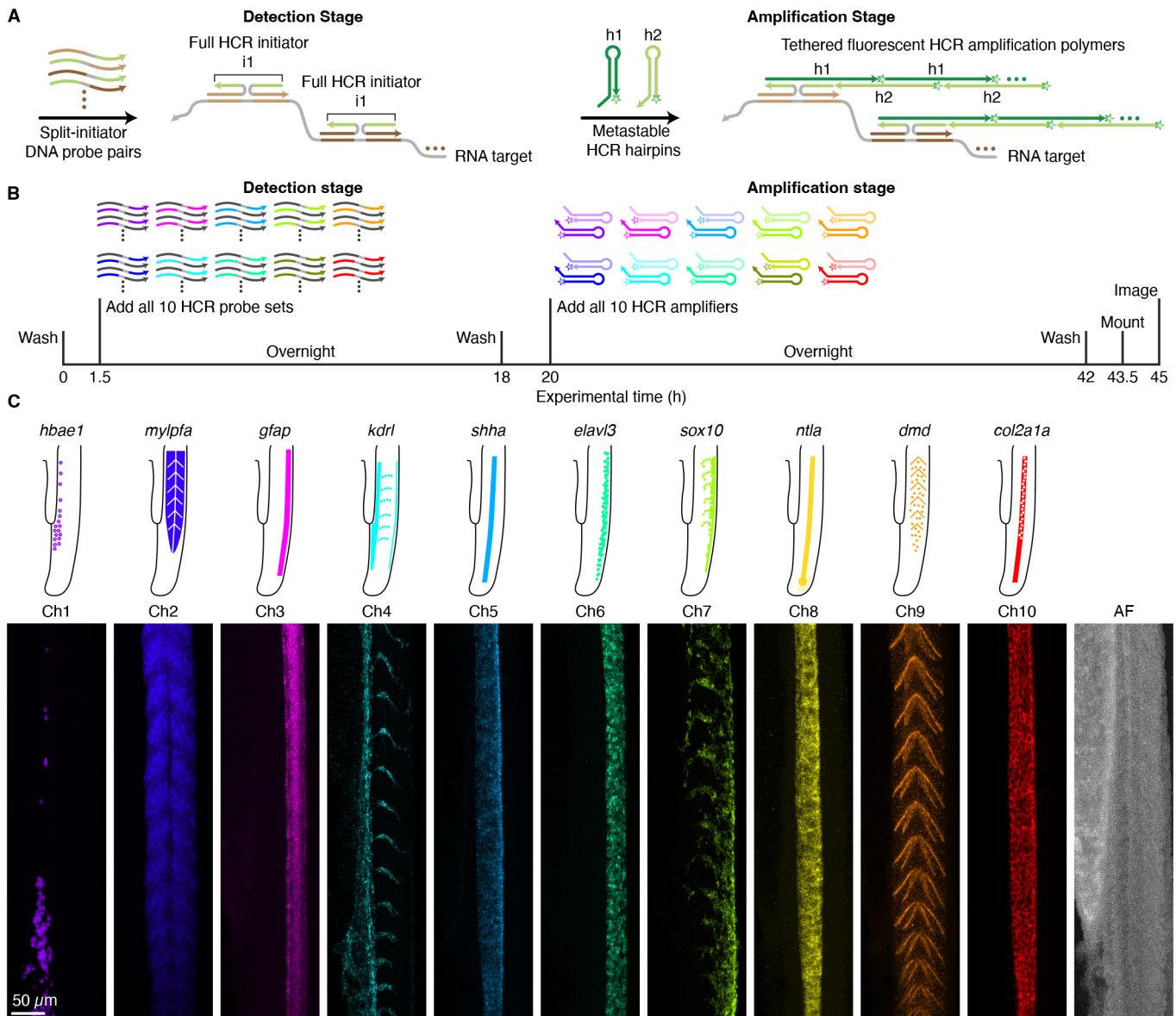


Fig. 2. 10-plex RNA imaging in a whole-mount zebrafish embryo. (A) Two-stage HCR RNA-FISH protocol. Detection stage: split-initiator DNA probe pairs bind to RNA targets to colocalize full HCR initiator *i1*; wash. Amplification stage: colocalized full initiator *i1* triggers self-assembly of fluorophore-labeled HCR hairpins into tethered fluorescent amplification polymers; wash. (B) 10-plex HCR RNA-FISH timeline. During the detection stage, all ten targets are detected in parallel. During the amplification stage, signal amplification is performed for all ten targets in parallel. (C) Top: Expression atlas for ten RNA targets in the tail of a zebrafish embryo (lateral view). Bottom: Linearly unmixed channels from a 10-plex confocal image including autofluorescence (AF) as an 11th channel; maximum intensity z-projections; $0.57 \times 0.57 \times 4.0$ μ m pixels. Embryo fixed at 27 hpf. See [Supplementary Information, Section S3.2 \(Figs S1-S8, Tables S7 and S8\)](#) and [Movie 1](#) for additional data.

To validate 10-plex HCR spectral imaging, we performed HCR RNA-FISH in whole-mount zebrafish embryos for ten target mRNAs with known expression patterns and a range of expression levels (Fig. 2C). Following the workflow of Fig. 1B, we prepared samples for 10-plex zebrafish replicates, as well as ten 1-plex reference samples, and two AF samples. One AF sample was used to determine the optimal excitation wavelength and detector wavelengths for autofluorescence. We spectrally imaged three replicate 10-plex samples (using probes and amplifiers for all ten targets) as well as 11 reference samples (a 1-plex sample for each of ten targets using a probe set and amplifier for only that target and an AF reference sample using no probes and amplifiers). Representative raw images are displayed in Figs S2-S4. Linear

unmixing then returned 11 unmixed channels (Fig. 2C; one channel per target plus an 11th AF channel). Visual inspection of the expression patterns revealed robust separation of all ten targets, including those with overlapping expression patterns [e.g. *shha*, *ntla* (*tbxta*) and *col2a1a* in the notochord; Moreno-Ayala et al., 2015]. High signal-to-background was achieved for all ten targets using ten fluorophores with overlapping spectra that span the visible and near-IR spectrum, including wavelengths with high autofluorescence. We estimated signal-to-background for each channel by characterizing signal plus background in a region of high expression and background in a region of no or low expression. This approach yields a conservative estimate of performance, as characterizing background in a region of little or no expression

places an upper bound on background and hence a lower bound on signal-to-background. Across the ten target mRNAs with expression levels estimated to vary by two orders of magnitude, the estimated signal-to-background ratio for each target ranged from 17 to 100 with a median of 46.5 (see [Table S8](#) for additional details).

10-plex qHCR imaging: mRNA relative quantitation with subcellular resolution in an anatomical context

We have previously demonstrated that HCR RNA-FISH and HCR IF enable accurate and precise relative quantitation of RNA and protein targets with subcellular resolution in an anatomical context (qHCR imaging mode), generating an amplified signal that scales approximately linearly with the number of target molecules per imaging voxel (Choi et al., 2018; Trivedi et al., 2018; Schwarzkopf et al., 2021). Here, we validate that spectral imaging and linear unmixing preserve the quantitative nature of HCR imaging. To test relative quantitation for all ten channels in a whole-mount zebrafish embryo, we redundantly detected each of five target mRNAs with two probe sets that each trigger a different HCR amplifier carrying a different fluorophore ([Fig. 3A](#)), leading to a ten-channel image with two channels for each of the five target mRNAs ([Fig. 3B](#)). If HCR signal scales approximately linearly with

the number of target mRNAs per voxel, a two-channel scatter plot of normalized voxel intensities for each target will yield a tight linear distribution with zero intercept (Trivedi et al., 2018). Consistent with expectation, we observed high accuracy (linearity with zero intercept) and precision (scatter around the line) for subcellular voxels for all five target mRNAs ([Fig. 3C](#)) and all ten channels. Moreover, all ten channels provided high signal-to-background ranging from 27 to 130 with a median of 60 (see [Table S11](#) for additional details).

dHCR imaging: digital mRNA absolute quantitation in a 10-plex sample

We have previously demonstrated that HCR enables digital mRNA absolute quantitation with single-molecule resolution for low-expression targets imaged at high magnification (dHCR imaging mode), enabling counting of individual target molecules as dots in highly autofluorescent samples, including whole-mount vertebrate embryos and thick brain slices (Shah et al., 2016a; Choi et al., 2018). We were curious whether spectral imaging and linear unmixing would preserve the single-molecule imaging capabilities of HCR imaging. To examine this question, we spectrally imaged the 10-plex redundant detection samples of [Fig. 3](#) again at high

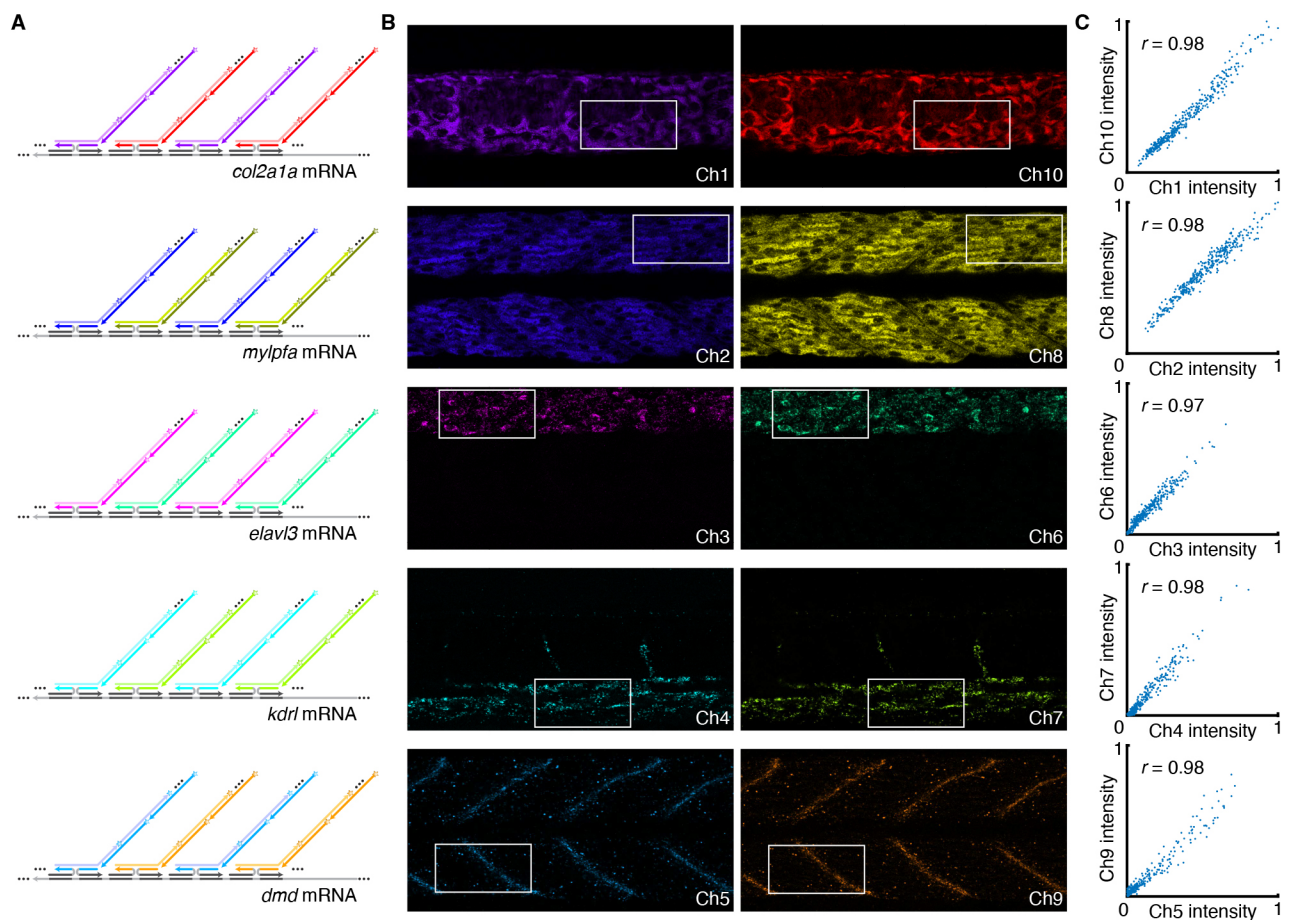


Fig. 3. 10-plex qHCR imaging: mRNA relative quantitation with subcellular resolution in an anatomical context using spectral imaging with linear unmixing. (A) Simultaneous two-channel redundant detection of each of five target mRNAs using a total of ten channels in a whole-mount zebrafish embryo. Each target mRNA is detected using two split-initiator DNA probe sets, each initiating an orthogonal HCR amplifier labeled with a different fluorophore. (B) Linearly unmixed channels from a 10-plex confocal image; single optical sections; $0.18 \times 0.18 \times 1.2 \mu\text{m}$ pixels. Embryo fixed at 27 hpf. (C) High accuracy (linearity with zero intercept) and precision (scatter around the line) for mRNA relative quantitation in an anatomical context. Highly correlated normalized signal (Pearson correlation coefficient, r) for subcellular voxels ($2.0 \times 2.0 \times 1.2 \mu\text{m}$) in the boxed regions in B. See [Supplementary Information, Section S3.3](#) (Figs S9-S19, Tables S7 and S9-S11) for additional data.

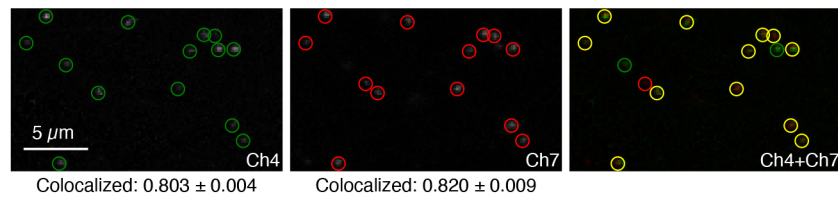


Fig. 4. dHCR imaging: Digital mRNA absolute quantitation in an anatomical context using 10-plex spectral imaging with linear unmixing. Two-channel redundant detection of target mRNA *kdr1* alongside two-channel redundant detection of four other target mRNAs as part of a 10-plex experiment in a whole-mount zebrafish embryo (see Fig. 3A). Linearly unmixed channels from a 10-plex confocal image in the dorsal posterior tail, where *kdr1* is expressed as single-molecule punctae. Representative field of view; maximum intensity z-projection; $0.18 \times 0.18 \times 1.2 \mu\text{m}$ pixels. Left: Ch4 (*kdr1*). Middle: Ch7 (*kdr1*). Right: Ch4+Ch7 merge. Green circles: dots detected in Ch4. Red circles: dots detected in Ch7. Yellow circles: dots detected in both channels. Colocalization represents the fraction of dots in one channel that are detected in both channels (mean \pm s.e.m., $n=3$ replicate embryos). Embryo fixed at 27 hpf. See Supplementary Information, Section S3.4 (Figs S20, S21, Table S12) for additional data.

magnification in the dorsal posterior region of the zebrafish tail, where the target mRNA *kdr1* is expressed as single-molecule punctae. In those samples, *kdr1* is redundantly detected in conjunction with redundant detection of four other target mRNAs.

To determine the fidelity with which single-molecule targets can be detected with spectral HCR imaging, we performed dot detection on the redundant *kdr1* channels (Ch4 and Ch7) using dot detection methods drawn from the computer vision community (Fig. 4). As false-positive and false-negative rates for each channel go to zero, the colocalization fraction for each channel (fraction of dots in a given channel that are in both channels) will approach one from below. We observed colocalization rates of ≈ 0.8 for both channels, roughly comparable to the performance observed in 2-plex experiments using bandpass HCR imaging (Choi et al., 2018), indicating that spectral imaging and linear unmixing are compatible with single-molecule imaging in 10-plex experiments.

10-plex RNA and protein imaging using spectral HCR RNA-FISH/IF in a mouse brain section

We have previously shown that HCR RNA-FISH/IF enables simultaneous multiplex, quantitative, high-resolution imaging of RNA and protein targets in highly autofluorescent samples (Schwarzkopf et al., 2021). To demonstrate the versatility of 10-plex HCR spectral imaging, here we image a total of seven mRNA targets and three protein targets in a coronal mouse brain section. HCR RNA-FISH/IF was performed using the three-stage protocol summarized in Fig. 5A. During the protein detection stage, protein targets are detected with unlabeled primary antibody probes that are subsequently detected by initiator-labeled secondary antibody probes. During the RNA detection stage, RNA targets are detected using split-initiator DNA probe sets. During the amplification stage, one-step HCR signal amplification is performed simultaneously for all ten RNA and protein targets. The same three-stage protocol is used to image any combination of up to ten RNA and protein targets simultaneously (Fig. 5B).

We used the workflow of Fig. 1B to perform HCR spectral imaging for a 10-plex sample as well as for 11 reference samples (one per fluorophore and one for autofluorescence). Representative raw images are displayed in Figs S23-S25. Linear unmixing returned 11 unmixed channels (Fig. 5C), one for each of seven target mRNAs, one for each of three target proteins, and one for autofluorescence. Each target RNA and protein has a characteristic expression pattern corresponding to certain cell types and/or cellular compartments within the cerebral cortex, enabling verification that fluorophores were successfully separated for all ten targets. For the protein targets, NFH (NEFH) labeled the intermediate filaments in large myelinated axons (Giasson and Mushynski, 1996), CD31

(PECAM1) labeled endothelial cells (Zhang et al., 2021) and RBFOX3 labeled neuronal nuclei (Lucas et al., 2014). Among the mRNA targets, *Actb* was expressed in several cell types (Wang et al., 2020), *Slc17a7* labeled excitatory neurons and *Gad1* labeled inhibitory neurons (Tasic et al., 2018). Subtypes of inhibitory neurons were labeled by *Sst* and *Vip*, and expression of these two mRNA targets overlapped as expected with *Gad1*-expressing neurons (Tasic et al., 2018); these results further confirmed the ability to distinguish targets with overlapping expression patterns using HCR spectral imaging with linear unmixing. Lastly, as expected, *Lamp5* expression was most pronounced in the upper layers of the cortex (Tiveron et al., 2016), and *Plp1* labeled oligodendrocytes, which are non-overlapping with the neuronal cells (Zeisel et al., 2015). Across ten RNA and protein targets, high signal-to-background was achieved for all targets, ranging from 25 to 140 with a median of 67.5 (see Table S13 for additional details).

DISCUSSION

HCR spectral imaging with linear unmixing enables researchers to simultaneously image any combination of ten RNA and protein targets without placing limitations on expression level (high/low) or pattern (overlapping/non-overlapping). The approach is well-suited for whole-mount vertebrate embryos and delicate specimens because the method does not employ repeated staining, imaging, registration and stripping to achieve multiplexing, so iterative sample degradation is avoided and there is no requirement for the sample to be immobilized on a slide during staining to facilitate registration, which is often infeasible for embryos and other complex samples. 10-plex HCR RNA-FISH (RNA targets only) or HCR IF (protein targets only) is achieved using a two-stage protocol involving two overnight incubations (detection stage, amplification stage). 10-plex HCR RNA-FISH/IF (combination of RNA and protein targets) is achieved using a three-stage protocol involving three overnight incubations (protein detection stage, RNA detection stage, amplification stage). All protocols are compatible with a normal sleep schedule.

Spectral imaging and linear unmixing preserve two complementary quantitative HCR imaging modes in the context of 10-plex experiments: (1) qHCR imaging – analog RNA or protein relative quantitation with subcellular resolution in an anatomical context (suitable for medium- or high-expression targets), (2) dHCR imaging – digital RNA absolute quantitation with single-molecule resolution in an anatomical context (suitable for low-expression targets). Multiplex HCR imaging enables bi-directional quantitative discovery (Trivedi et al., 2018): ‘read-out’ from anatomical space to expression space to discover co-expression relationships in selected regions of the sample; ‘read-in’ from expression space to anatomical

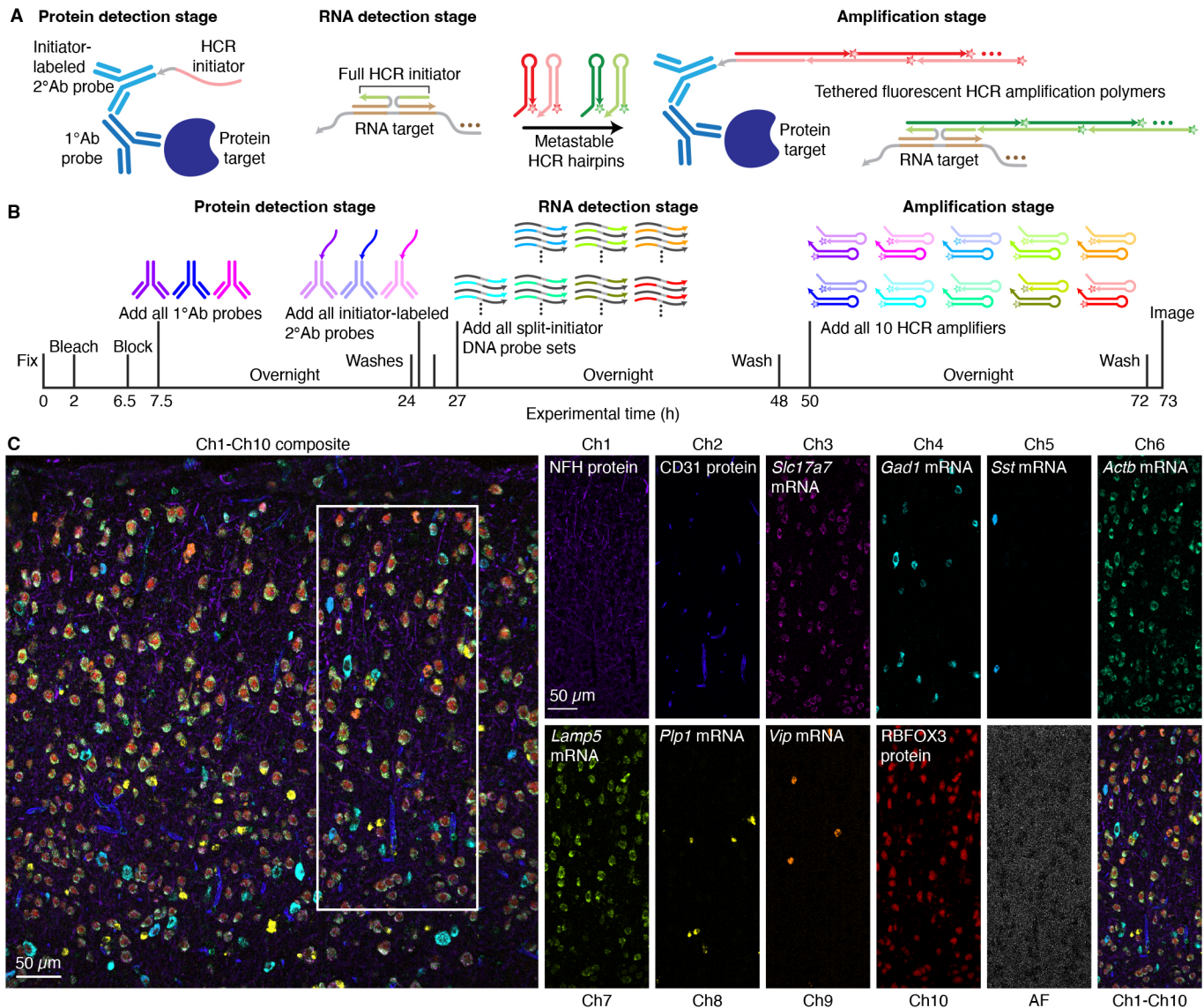


Fig. 5. 10-plex RNA and protein imaging in a fresh-frozen mouse brain section. (A) Three-stage HCR RNA-FISH/IF protocol. Protein-detection stage: unlabeled primary antibody probes bind to protein targets; initiator-labeled secondary antibody probes bind to primary antibody probes; wash. RNA-detection stage: split-initiator DNA probes bind to RNA targets; wash. Amplification stage: initiators trigger self-assembly of fluorophore-labeled HCR hairpins into tethered fluorescent amplification polymers; wash. (B) 10-plex HCR RNA-FISH/IF timeline. During the protein-detection stage, all protein targets are detected in parallel. During the RNA-detection stage, all RNA targets are detected in parallel. During the amplification stage, signal amplification is performed for all ten targets in parallel. (C) 10-plex confocal image of three protein targets and seven mRNA targets in the cerebral cortex of a fresh-frozen mouse brain section; single optical section; $0.57 \times 0.57 \times 4.0 \mu\text{m}$ pixels. Left: Composite image of linearly unmixed Ch1-Ch10. Right: Single fluorescence channels for the boxed region in the composite image [including autofluorescence (AF) as an 11th channel]. Sample: fresh-frozen mouse brain section (coronal); $5 \mu\text{m}$ thickness; interaural region $0.88 \text{ mm} \pm 0.20 \text{ mm}$; 8 weeks old. See [Supplementary Information, Section S3.5 \(Figs S22-S33, Tables S7 and S13\)](#) for additional data.

space to discover those anatomical locations in which selected gene co-expression relationships occur. Here, by using HCR spectral imaging and linear unmixing to achieve 10-plex, high-accuracy, high-precision, high-resolution qHCR imaging, we enable 10-dimensional quantitative read-out/read-in analyses for any combination of ten RNA and/or protein circuit elements in the anatomical context of highly autofluorescent samples. Note that in performing these quantitative co-expression analyses, a 4-plex experiment enables exploration of six target pairs and a 5-plex experiment enables exploration of ten target pairs, but a 10-plex experiment enables exploration of 45 target pairs, all in the anatomical context of a single sample.

To detect protein targets, the present work performs HCR IF using unlabeled primary antibody probes and initiator-labeled secondary antibody probes, thereby requiring that each primary antibody be of a different isotype or raised in a different host species, which is sometimes feasible given the large libraries of commercially available antibodies. For example, we demonstrate imaging of three protein targets simultaneously using unlabeled chicken, rat and rabbit primary antibody probes (Fig. 5). However, in situations where it is desirable to use multiple primary antibodies raised in the same host species or of the same isotype, HCR IF can instead be performed using initiator-labeled primary antibody probes (Schwarzkopf et al., 2021). Antibody-oligo conjugation can

sometimes interfere with target recognition, necessitating post-conjugation probe validation. By contrast, using a small library of validated initiator-labeled secondary antibodies as we do here, primary antibodies can be exploited without modification, eliminating the need to validate antibody-oligo conjugation for each new target protein.

For RNA targets, HCR imaging provides automatic background suppression throughout the protocol, ensuring that reagents will not generate amplified background even if they bind non-specifically in the sample (Choi et al., 2018). During the detection stage, split-initiator DNA probes that bind non-specifically in the sample do not colocalize a full HCR initiator and do not trigger HCR. During the amplification stage, metastable HCR hairpins that bind non-specifically do not trigger formation of an amplification polymer. For protein targets, HCR hairpins continue to provide automatic background suppression during the amplification stage, but the detection stage employs antibody probes that carry a full HCR initiator so it is important to use antibodies that are highly selective for their targets and to wash unused antibody probes from the sample. High signal-to-background is achieved across all ten channels for both RNA and protein targets.

Once sample preparation and wash conditions have been validated to enable 1-plex HCR imaging with high signal-to-background in a given sample type, the goal of the present work is to provide a standardized set of ingredients to enable plug-and-play 10-plex HCR spectral imaging: ten orthogonal HCR amplifiers (one per target), an optimized set of ten fluorophores (one per amplifier), ten optimized excitation wavelengths (one per fluorophore), ten sets of optimized detection wavelengths (one to three detectors per fluorophore), an optimized excitation wavelength and set of four detection wavelengths for autofluorescence (measured by the user for the sample type of interest; treated as an 11th channel), spectral imaging hardware that provides the flexibility to use optimal excitation wavelengths for each fluorophore and for autofluorescence (Leica Stellaris 8 confocal microscope), and linear unmixing software (Leica LAS X or Unmix 1.0) that returns 11 unmixed channels (one per fluorophore and one for autofluorescence).

When assigning targets to Ch1-Ch10, higher-expression targets were assigned to channels that employ fluorophores with emission spectra strongly overlapping sample autofluorescence (e.g. Ch1-Ch3 for whole-mount zebrafish embryos and fresh-frozen mouse brain sections) or with emission spectra for which the microscope detectors are less sensitive (e.g. Ch10 in the near-IR wavelength range using the Leica Stellaris 8 confocal microscope). Other than these precautions, the targets were assigned randomly to channels without taking into consideration the expression level of each target or the degree of spatial overlap between expression patterns.

For users that do not have access to a Leica Stellaris 8 microscope, our robust ingredients and workflow provide a starting point for adaptation to locally available hardware and our Unmix 1.0 software provides the flexibility to unmix spectral imaging data without the use of Leica LAS X software. If a user encounters a sample in which different tissues produce widely differing autofluorescence spectra, the number of auxiliary autofluorescence channels can be increased, collecting one AF reference spectrum per AF channel.

These standardized ingredients are combined in a straightforward workflow. To perform 10-plex HCR spectral imaging in a highly autofluorescent sample, a user need only image a reference spectrum for each fluorophore in a 1-plex sample and an autofluorescence reference spectrum in an unlabeled sample in order to linearly unmix the spectral fluorescence of a 10-plex sample.

MATERIALS AND METHODS

Probes, amplifiers and buffers

Details regarding the probes, amplifiers and buffers for each experiment are displayed in [Table S1](#) for HCR RNA-FISH and [Table S2](#) for HCR IF.

10-plex HCR spectral imaging and linear unmixing

10-plex HCR spectral imaging and linear unmixing were performed using the protocol detailed in [Supplementary Information, Section S2.1](#) (including [Tables S5 and S6](#)). Linear unmixing was performed using Leica LAS X software for main text figures. Alternatively, linear unmixing can be performed with our Unmix 1.0 software package (as demonstrated in [Figs S7, S8 and S30-S33](#); available for download from Molecular Technologies (<https://www.moleculartechnologies.org/>), a non-profit academic resource within the Beckman Institute at Caltech.

HCR RNA-FISH in whole-mount zebrafish embryos

Within the 10-plex workflow, HCR RNA-FISH in whole-mount zebrafish embryos was performed using the protocols detailed in [Supplementary Information, Section S2.2](#). Experiments were performed in AB wild-type whole-mount zebrafish embryos [fixed at 27 hours post-fertilization (hpf)] obtained from the Zebrafish Facility within the Beckman Institute at Caltech, CA, USA. Procedures for the care and use of zebrafish embryos were approved by the Caltech Institutional Animal Care & Use Committee.

HCR RNA-FISH/IF in fresh-frozen mouse brain sections

Within the 10-plex workflow, HCR RNA-FISH/IF in fresh-frozen mouse brain sections was performed using the protocols detailed in [Supplementary Information, Section S2.3](#). Experiments were performed in C57BL/6 fresh-frozen coronal mouse brain sections (thickness: 5 μ m; region: interaural 0.88 mm \pm 0.2 mm; age: 8 weeks old; sex: male) from Acepix Biosciences (A2203-0561).

Confocal microscopy

Microscopy was performed using a Leica Stellaris 8 inverted confocal microscope with an HC PL APO 20 \times /0.75 IMM CORR CS2 (11506343) objective or HC PL APO 63 \times /1.40 OIL CS2 (11506350) objective. Details on the objectives, excitation wavelengths, detectors and detection wavelengths used for each experiment are displayed in [Table S3](#).

Image analysis

Image analysis was performed as detailed in [Supplementary Information, Section S1.4](#), including: definition of raw pixel intensities; measurement of signal, background, and signal-to-background; calculation of normalized subcellular voxel intensities for qHCR imaging; and dot detection and colocalization for dHCR imaging. Dot detection and colocalization were performed with our Dot Detection 2.0 software package (using the parameters in [Table S4](#)) available for download from Molecular Technologies (<https://www.moleculartechnologies.org/>). For qHCR redundant detection experiments ([Fig. 3](#); see [Supplementary Information, Section S3.3](#)), Huygens Software (Scientific Volume Imaging) was used to correct for chromatic aberration across the ten channels. All linearly unmixed images are displayed with 0.1% of pixels saturated across three replicates, with the exception of the single-molecule images of [Fig. 4](#) and [Fig. S20](#), which are displayed with no saturated pixels. All images are displayed without background subtraction.

Acknowledgements

We thank A. Kahan of the V. Gradinaru Lab for the gift of mouse brain sections during initial validation; M. E. Bronner for reading a draft of the manuscript; and the following resources within the Beckman Institute at Caltech: Molecular Technologies for providing HCR reagents, G. Spigolon of the Biological Imaging Facility for assistance with imaging, and the Zebrafish Facility for providing zebrafish embryos. The Leica Stellaris 8 confocal microscope in the Biological Imaging Facility within the Beckman Institute at Caltech was purchased with support from Caltech and the following Caltech entities: the Beckman Institute, the Resnick Sustainability Institute, the Division of Biology & Biological Engineering, and the Merkin Institute for Translational Research.

Competing interests

The authors declare competing financial interests in the form of patents, pending patent applications, and the startup company Molecular Instruments, Inc.

Author contributions

Conceptualization: N.A.P.; Methodology: S.J.S., M.E.F., N.A.P.; Software: M.E.F.; Validation: S.J.S., M.E.F., J.K.H.; Investigation: S.J.S., J.K.H., G.J.S.; Writing - original draft: S.J.S., N.A.P.; Writing - review & editing: S.J.S., M.E.F., J.K.H., G.J.S., N.A.P.; Visualization: S.J.S., M.E.F.; Supervision: N.A.P.; Project administration: N.A.P.; Funding acquisition: N.A.P.

Funding

This work was funded by the National Institute of Biomedical Imaging and Bioengineering (R01EB006192), a National Institute of General Medical Sciences training grant (GM008042 to S.J.S.) and the Beckman Institute, California Institute of Technology (PMTIC). Open Access funding provided by California Institute of Technology. Deposited in PMC for immediate release.

Data availability

All relevant data can be found within the article and its [supplementary information](#).

References

- Acloque, H., Wilkinson, D. G. and Nieto, M. A.** (2008). In situ hybridization analysis of chick embryos in whole-mount and tissue sections. In *Avian Embryology*, 2nd edn. (ed. M. Bronner-Fraser), pp. 169-185. San Diego, CA: Elsevier Academic Press.
- Ahnfelt-Rønne, J., Jørgensen, M. C., Hald, J., Madsen, O. D., Serup, P. and Hecksher-Sørensen, J.** (2007). An improved method for three-dimensional reconstruction of protein expression patterns in intact mouse and chicken embryos and organs. *J. Histochem. Cytochem.* **55**, 925-930. doi:10.1369/jhc.7A7226.2007
- Barroso-Chinea, P., Aymerich, M. S., Castle, M. M., Pérez-Manzo, M., Tuñón, T., Erro, E. and Lanciego, J. L.** (2007). Detection of two different mRNAs in a single section by dual in situ hybridization: A comparison between colorimetric and fluorescent detection. *J. Neurosci. Methods* **162**, 119-128. doi:10.1016/j.jneumeth.2006.12.017
- Chan, P. M., Yuen, T., Ruf, F., Gonzalez-Maeso, J. and Sealfon, S. C.** (2005). Method for multiplex cellular detection of mRNAs using quantum dot fluorescent in situ hybridization. *Nucleic Acids Res.* **33**, e161. doi:10.1093/nar/gni162
- Chen, K. H., Boettiger, A. N., Moffitt, J. R., Wang, S. and Zhuang, X.** (2015). Spatially resolved, highly multiplexed RNA profiling in single cells. *Science* **348**, aaa6090. doi:10.1126/science.aaa6090
- Choi, H. M. T., Chang, J. Y., Trinh, L. A., Padilla, J. E., Fraser, S. E. and Pierce, N. A.** (2010). Programmable in situ amplification for multiplexed imaging of mRNA expression. *Nat. Biotechnol.* **28**, 1208-1212. doi:10.1038/nbt.1692
- Choi, H. M. T., Beck, V. A. and Pierce, N. A.** (2014). Next-generation in situ hybridization chain reaction: Higher gain, lower cost, greater durability. *ACS Nano* **8**, 4284-4294. doi:10.1021/nn405717p
- Choi, H. M. T., Calvert, C. R., Husain, N., Huss, D., Barsi, J. C., Deverman, B. E., Hunter, R. C., Kato, M., Lee, S. M., Abelin, A. C. T. et al.** (2016). Mapping a multiplexed zoo of mRNA expression. *Development* **143**, 3632-3637. doi:10.1242/dev.140137
- Choi, H. M. T., Schwarzkopf, M., Fornace, M. E., Acharya, A., Artavanis, G., Stegmaier, J., Cunha, A. and Pierce, N. A.** (2018). Third-generation in situ hybridization chain reaction: multiplexed, quantitative, sensitive, versatile, robust. *Development* **145**, dev165753. doi:10.1242/dev.165753
- Clay, H. and Ramakrishnan, L.** (2005). Multiplex fluorescent in situ hybridization in zebrafish embryos using tyramide signal amplification. *Zebrafish* **2**, 105-111. doi:10.1089/zeb.2005.2.105
- Coons, A. H., Creech, H. J. and Jones, R. N.** (1941). Immunological properties of an antibody containing a fluorescent group. *Proc. Soc. Exp. Biol. Med.* **47**, 200-202. doi:10.3181/00379727-47-13084P
- Cutrale, F., Trivedi, V., Trinh, L. A., Chiu, C.-L., Choi, J. M., Artiga, M. S. and Fraser, S. E.** (2017). Hyperspectral phasor analysis enables multiplexed 5D in vivo imaging. *Nat. Methods* **14**, 149-152. doi:10.1038/nmeth.4134
- Cutrale, F., Fraser, S. E. and Trinh, L. A.** (2019). Imaging, visualization, and computation in developmental biology. *Annu. Rev. Biomed. Data Sci.* **2**, 223-251. doi:10.1146/annurev-biodatasci-072018-021305
- Denkers, N., García-Villalba, P., Rodesch, C. K., Nielson, K. R. and Mauch, T. J.** (2004). FISHing for chick genes: triple-label whole-mount fluorescence in situ hybridization detects simultaneous and overlapping gene expression in avian embryos. *Dev. Dyn.* **229**, 651-657. doi:10.1002/dvdy.20005
- Dirks, R. M. and Pierce, N. A.** (2004). Triggered amplification by hybridization chain reaction. *Proc. Natl. Acad. Sci. U. S. A.* **101**, 15275-15278. doi:10.1073/pnas.0407024101
- Femino, A. M., Fay, F. S., Fogarty, K. and Singer, R. H.** (1998). Visualization of single RNA transcripts in situ. *Science* **280**, 585-590. doi:10.1126/science.280.5363.585
- Fujisawa, S., Yarilin, D., Fan, N., Turkekul, M., Xu, K., Barlas, A. and Manova-Todorova, K.** (2015). Understanding the three-dimensional world from two-dimensional immunofluorescent adjacent sections. *J. Pathol. Inform.* **6**, 27. doi:10.4103/2153-3539.158052
- Garini, Y., Young, I. T. and McNamara, G.** (2006). Spectral imaging: principles and applications. *Cytom. A* **69**, 735-747. doi:10.1002/cyto.a.20311
- Ghoddousi, R. A. M., Magalong, V. M., Kamitakahara, A. K. and Levitt, P.** (2022). SCAMPR, a single-cell automated multiplex pipeline for RNA quantification and spatial mapping. *Cell Rep. Methods* **2**, 100316. doi:10.1016/j.crmeth.2022.100316
- Giasson, B. I. and Mushynski, W. E.** (1996). Aberrant stress-induced phosphorylation of perikaryal neurofilaments. *J. Biol. Chem.* **271**, 30404-30409. doi:10.1074/jbc.271.48.30404
- Glass, G., Papin, J. A. and Mandell, J. W.** (2009). SIMPLE: a sequential immunoperoxidase labeling and erasing method. *J. Histochem. Cytochem.* **57**, 899-905. doi:10.1369/jhc.2009.953612
- Harland, R. M.** (1991). In situ hybridization: an improved whole-mount method for *Xenopus* embryos. *Methods Cell Biol.* **36**, 685-695. doi:10.1016/S0091-679X(08)60307-6
- Harrison, P. R., Conkie, D., Paul, J. and Jones, K.** (1973). Localisation of cellular globin messenger RNA by in situ hybridisation to complementary DNA. *FEBS Lett.* **32**, 109-112. doi:10.1016/0014-5793(73)80749-5
- Kennedy-Darling, J., Bhate, S. S., Hickey, J. W., Black, S., Barlow, G. L., Vazquez, G., Venkatarahaman, V. G., Samusik, N., Goltsev, Y., Schürch, C. M. et al.** (2021). Highly multiplexed tissue imaging using repeated oligonucleotide exchange reaction. *Eur. J. Immunol.* **51**, 1262-1277. doi:10.1002/eji.202048891
- Kerstens, H. M., Poddighe, P. J. and Hanselaar, A. G.** (1995). A novel *in-situ* hybridization signal amplification method based on the deposition of biotinylated tyramine. *J. Histochem. Cytochem.* **43**, 347-352. doi:10.1177/43.4.7897179
- Kim, S.-W., Roh, J. and Park, C.-S.** (2016). Immunohistochemistry for pathologists: protocols, pitfalls, and tips. *J. Pathol. Transl. Med.* **50**, 411-418. doi:10.4132/jptm.2016.08.08
- Kishi, J. Y., Lapan, S. W., Beliveau, B. J., West, E. R., Zhu, A., Sasaki, H. M., Saka, S. K., Wang, Y., Cepko, C. L. and Yin, P.** (2019). SABER amplifies FISH: enhanced multiplexed imaging of RNA and DNA in cells and tissues. *Nat. Methods* **16**, 533-544. doi:10.1038/s41592-019-0404-0
- Kislauskis, E. H., Li, Z., Singer, R. H. and Taneja, K. L.** (1993). Isoform-specific 3'-untranslated sequences sort α -cardiac and β -cytoplasmic actin messenger RNAs to different cytoplasmic compartments. *J. Cell Biol.* **123**, 165-172. doi:10.1083/jcb.123.1.165
- Koh, J., Kwak, Y., Kim, J. and Kim, W. H.** (2019). High-throughput multiplex immunohistochemical imaging of the tumor and its microenvironment. *Cancer Res. Treat.* **52**, 98-108. doi:10.4143/crt.2019.195
- Kosman, D., Mizutani, C. M., Lemons, D., Cox, W. G., McGinnis, W. and Bier, E.** (2004). Multiplex detection of RNA expression in *Drosophila* embryos. *Science* **305**, 846. doi:10.1126/science.1099247
- Lehmann, R. and Tautz, D.** (1994). In situ hybridization to RNA. In *Drosophila melanogaster: Practical Uses in Cell and Molecular Biology* (ed. L. S. B. Goldstein and E. A. Fyrberg), pp. 575-598. San Diego, CA: Elsevier Academic Press.
- Lignell, A., Kerosuo, L., Streichan, S. J., Cai, L. and Bronner, M. E.** (2017). Identification of a neural crest stem cell niche by spatial genomic analysis. *Nat. Commun.* **8**, 1830. doi:10.1038/s41467-017-01561-w
- Lubeck, E., Coskun, A. F., Zhiyentayev, T., Ahmad, M. and Cai, L.** (2014). Single-cell in situ RNA profiling by sequential hybridization. *Nat. Methods* **11**, 360-361. doi:10.1038/nmeth.2892
- Lucas, C.-H., Calvez, M., Babu, R. and Brown, A.** (2014). Altered subcellular localization of the NeuN/Rbfox3 RNA splicing factor in HIV-associated neurocognitive disorders (HAND). *Neurosci. Lett.* **558**, 97-102. doi:10.1016/j.neulet.2013.10.037
- Mansfield, J. R., Hoyt, C. and Levenson, R. M.** (2008). Visualization of microscopy-based spectral imaging data from multi-label tissue sections. *Curr. Protoc. Mol. Biol.* **84**, 14.19.1-14.19.15. doi:10.1002/0471142727.mb1419s84
- Mitchell, R. T., Camacho-Moll, M. E., Macdonald, J., Anderson, R. A., Kelnar, C. J. H., O'Donnell, M., Sharpe, R. M., Smith, L. B., Grigor, K. M., Wallace, W. H. B. et al.** (2014). Intratubular germ cell neoplasia of the human testis: heterogeneous protein expression and relation to invasive potential. *Mod. Pathol.* **27**, 1255-1266. doi:10.1038/modpathol.2013.246
- Moffitt, J. R., Hao, J., Wang, G., Chen, K. H., Babcock, H. P. and Zhuang, X.** (2016). High-throughput single-cell gene-expression profiling with multiplexed error-robust fluorescence in situ hybridization. *Proc. Natl. Acad. Sci. USA* **113**, 11046-11051. doi:10.1073/pnas.1612826113
- Moreno-Ayala, R., Schnabel, D., Salas-Vidal, E. and Lomelí, H.** (2015). PIAS-like protein Zimp7 is required for the restriction of the zebrafish organizer and mesoderm development. *Dev. Biol.* **403**, 89-100. doi:10.1016/j.ydbio.2015.04.013
- Nieto, M. A., Patel, K. and Wilkinson, D. G.** (1996). In situ hybridization analysis of chick embryos in whole mount and tissue sections. In *Methods in Avian Embryology* (ed. M. Bronner-Fraser), pp. 219-235. San Diego, CA: Elsevier Academic Press.

